



CHORUS

This is the accepted manuscript made available via CHORUS. The article has been published as:

Substrate-supported large-band-gap quantum spin Hall insulator based on III-V bismuth layers

J. E. Padilha, A. Janotti, A. Fazzio, and A. J. R. da Silva

Phys. Rev. B **94**, 195424 — Published 16 November 2016

DOI: [10.1103/PhysRevB.94.195424](https://doi.org/10.1103/PhysRevB.94.195424)

Substrate-supported large band gap quantum spin Hall insulator based on III-V bismuth layers

J. E. Padilha,^{1,*} A. Janotti,^{2,†} A. Fazzio,^{3,4,‡} and A. J. R. da Silva^{3,5,§}

¹*Campus Avançado Jandaia do Sul, Universidade Federal do Paraná, 86900-000, Jandaia do Sul, PR, Brazil*

²*Department of Materials Science & Engineering,*

University of Delaware, Newark, Delaware 19716-3106, USA.

³*Instituto de Física, Universidade de São Paulo, CP 66318, 05315-970, São Paulo, SP, Brazil.*

⁴*Centro de Ciências Naturais e Humanas, Universidade Federal do ABC, Santo André, São Paulo, Brazil 09210-170.*

⁵*Laboratório Nacional de Luz Síncrotron*

We show that III-V bismuth-based 2D materials grown on anion-terminated SrTe (111) substrate are 2D topological insulators. The III-Bi layers exhibit large non-trivial band gaps, ranging from 0.15 to 0.72 eV, depending on the passivation on the top surface, i.e., using hydrogen or halogens. We find that Γ -centered Dirac helical states, protected by time-reversal symmetry, appear at the edges of nanoribbon structures made of III-Bi layers on the SrTe substrate. The non-trivial character of the band gap is also determined by calculations of the Z_2 invariant. We also find that the topological phase is maintained in ultra-thin quantum well heterostructures SrTe/III-Bi/SrTe, i.e., when the 2D materials are sandwiched between SrTe along the [111] direction, opening a new route for the fabrication of nanostructured devices based on 2D quantum spin Hall insulators.

PACS numbers: 71.70.Ej, 63.50.Gh, 71.15.Nc, 73.22.??

Two dimensional topological insulators (2D TI), also known as quantum spin Hall insulators (QSHI), are promising materials for spintronics and nanoelectronics. These materials display an insulating bulk and spin-polarized gapless edge states with a conical energy dispersion. The edge states are protected against perturbations that preserves time reversal symmetry, preventing backscattering. The QSHI phase was first proposed to occur in graphene by Kane and Mele¹. However, due to the very small spin-orbit induced band gap in graphene, the QSHI phase is expected to occur only at extremely low temperatures^{2,3}, making it difficult to probe in a controllable manner.

The QSHI phase was first observed in HgTe/CdTe quantum well structures⁴, yet the observed band gap of 5 meV is too small for practical applications. Other materials systems have also been proposed for the observation of the QSHI phase, such as silicene, with gap of 1.9 meV^{5,6}, germanene (gap of 29 meV)^{6,7}, stanene (0.1 eV) and its halogenated forms (up to 0.34 eV)⁸. The spin-orbit interaction is a key feature in topological insulators, raising the interest in heavy elements, such as bismuth, as building blocks of these materials. In fact, Bi is responsible for the high spin-orbit coupling that drives the band inversion in Bi₂Se₃ and Bi₂Te₃⁹⁻¹¹. Bismuth layers have also been proposed to present the quantum spin hall effect^{12,13}.

Motivated by the use of bismuth as source of high spin-orbit coupling (SOC) strength, III-Bi binary compounds have been proposed, by Chuang et al.¹⁴, as a new class of large band-gap 2D quantum spin Hall insulators. Their halogenated form¹⁵⁻¹⁷, together with the fluorinated PbX binary compounds proposed by Padilha et al.¹⁸, are 2D topological insulators with largest non-trivial band gaps to our knowledge. However, these 2D QSHI were proposed to exist in a free-standing form, which is quite chal-

lenging to achieve in practice. The growth of 2D topological insulators on substrates that preserve their topological properties is yet to be demonstrated, and would pave the way to more realistic approaches and practical applications.

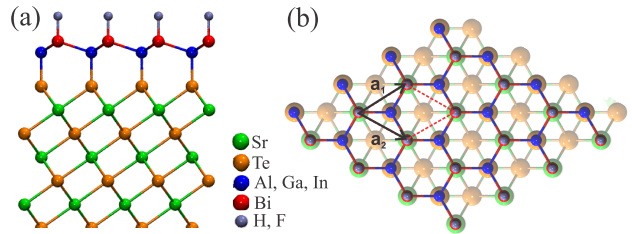


FIG. 1. (Color online) (a) Side view and (b) top view of the Te-terminated SrTe(111)/III-Bi-X heterostructure, with III: Al, Ga, Bi and X= H, F, Cl, Br, I. The unit cell is defined by the vectors \mathbf{a}_1 and \mathbf{a}_2 .

Having the 2D material supported on a substrate is not only more practical than 2D free standing layers, it could also provide new ways to control the topological properties, and add flexibility to device design. For instance, the substrate could impose strain to the 2D TI, which allows for tuning the non-trivial band gap in 2D systems¹⁹. However, there are some requirements from the interaction of the 2D TI with the substrate that must be fulfilled in order to preserve the topological phase: The substrate should have a large band gap, and the band alignment between the substrate and the 2D material should be of type II for an effective separation of the topological states in the TI and the trivial states in the substrate. Furthermore, the substrate should not induce metallic surface states near the Fermi level of the 2D material²⁰. These requirements point to highly ionic,

very large band gap insulators as substrates, so that surface states appear only close to the band edges and are readily passivated. In this context, Xu *et al.*²¹ have recently showed that stanene could be either a trivial or a QSH, depending of the substrate, and that other properties such as the Rashba splitting could be controlled by the lattice parameter of the substrate. III-Bi materials were previously proposed to be grown on the Si(111) surface^{22,23}. Here we propose the growth of III-Bi ultrathin layers on SrTe. The small lattice mismatch between SrTe and the III-Bi compounds facilitates growth, and the much larger band gap of SrTe, compared to Si, will avoid possible conduction through the substrate material.

In this work we show that III-Bi 2D materials grown on anion-terminated SrTe (111) are 2D topological insulators when the exposed surface are passivated with hydrogen or halogens. These materials display large non-trivial band gaps, ranging from 0.15 to 0.72 eV. Our calculations show that Γ -centered 1D Dirac helical states, protected by time-reversal symmetry, appear at the edges of III-Bi nanoribbon structures. We also find that there is no interference between the Dirac helical states with the states from the SrTe substrate, which is a trivial insulator with very large band gap. Finally, we show that when these 2D materials are sandwiched between thick SrTe layers, such as in a ultrathin SrTe/III-Bi/SrTe quantum well heterostructures, the topological phase remains intact. These results open a new route to build nanoscale devices based on 2D quantum spin hall insulators.

I. METHODS

Our calculations are based on density functional theory^{24,25}, as implemented in the VASP code²⁸. We use projector augmented wave potentials²⁹ and plane-wave basis set with energy cutoff of 500 eV. The Brillouin zone is sampled with a $9 \times 9 \times 1$ k -point mesh. The III-Bi (III=Al, Ga, Bi) layer on the SrTe substrate is simulated using a periodic slab with 15 Å of vacuum. Dipole corrections between the images were included in all calculations. To avoid problems of having different surfaces on top and bottom of the slab, we employed a symmetric slab, as also used by Xu *et al.*²¹ for stanene grown on a substrate. The slabs consist of 13 atomic layers of substrate with the inner seven layers fixed at the bulk crystal structure, and two equivalent top and bottom surfaces covered by III-Bi. Except for the seven inner layers of the SrTe substrate, that were kept fixed during the relaxation process, all other atoms were fully relaxed until the force on each atom was smaller than 0.001 eV/Å. Since the materials addressed here do not present inversion symmetry, in order to verify the topological character of the systems, we determine the Z_2 invariant based on the evolution of the Wannier Center of Charges (WCCs) method, as proposed by Soluyanov and Vanderbilt^{30,31}. This method is based on Wannier

Functions described as:

$$|Rn\rangle = \frac{i}{2\pi} \int_{-\pi}^{\pi} dk e^{ik(R-x)} |u_{nk}\rangle \quad (1)$$

The WF depend on a gauge choice for the Bloch states $|u_{nk}\rangle$. Following Marzari and Vanderbilt description³², to optimally localized the WF, we define WCCs as the mean value of the position operator $\bar{x}_n = \langle 0n | \hat{X} | 0n \rangle$. In this way the Z_2 can be written as:

$$Z_2 = \left[\sum_{\alpha} \bar{x}_{\alpha}^I(TRIM_1) - \bar{x}_{\alpha}^{II}(TRIM_1) \right] - \left[\sum_{\alpha} \bar{x}_{\alpha}^I(TRIM_2) - \bar{x}_{\alpha}^{II}(TRIM_2) \right] \quad (2)$$

With α band index of the occupied states, II and I being the Kramer partners. The Z_2 invariant can be obtained by counting the even or odd number of crossings of any arbitrary horizontal reference line. When the WCC evolution curves cross any arbitrary reference lines odd times, $Z_2 = 1$. For the ribbon structures, due to the large number of atoms and electrons, we used the OpenMX code³³ for band structure calculations since it is more computationally efficient than VASP, yet equally accurate.

II. RESULTS AND DISCUSSIONS

In Figure 1(a) and (b) we show a side view and top view of the model structure considered in our calculations. As substrate we used rock salt anion-terminated SrTe(111). SrTe has a experimental lattice parameter of 4.711 Å, which is close to the in-plane lattice parameters of the III-Bi layers¹⁴⁻¹⁷. In the free-standing form, only the InBi system is mechanically stable, i.e., it has no imaginary modes in the phonon spectra, whereas the Al and Ga materials exhibit low energy imaginary modes. However, this instability is avoided when the system is grown on a substrate. We find that the lowest-energy configuration for the SrTe/III-Bi interface consists of having the column-III atoms on top of the Te atoms, as shown in Figure 1, and the Bi atoms on top of the cation site, as in a *hcp* lattice stacking. We find that the *fcc* lattice stacking is 0.05 eV higher in energy. Our calculations show that these two interfaces have similar electronic properties. All the other possible configurations are higher in energy.

The band structures of AlBi, GaBi, and InBi on the SrTe substrate are shown in Figures 2(a), (b) and (c). The shaded region stands for the band structure without spin-orbit coupling (SOC) and the blue lines is when the SOC is turned on. We note that the three systems exhibit a semimetallic character, with the presence of partially occupied states near the Fermi level, around the Γ point. These states are mostly composed of unsaturated p_z orbitals from the Bi atoms in the exposed surface.

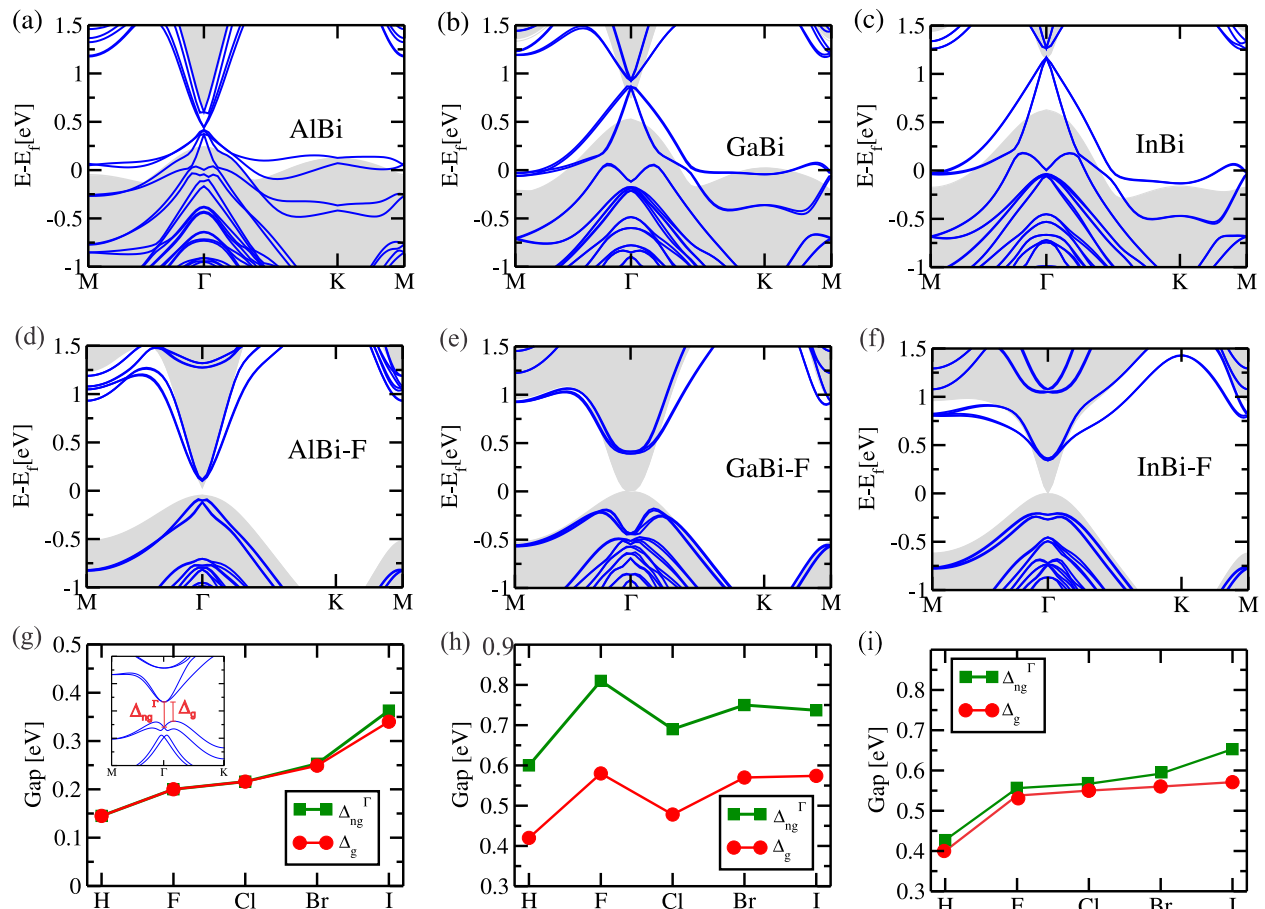


FIG. 2. (Color online) Band structures of (a) AlBi, (b) GaBi, (c) InBi, (d) AlBi-F, (e) GaBi-F and (f) InBi-F on Te-terminated SrTe(111). The gray regions stand for band structures without spin-orbit coupling (SOC), and the blue lines stand for bands with SOC. Evolution of the band gap of III-Bi-X as function of X (X=H, F, Cl, Br, I) are shown in (g) AlBi-X, (h) GaBi-X and (i) InBi-X. The metallic, pristine case is not shown. The red circles represent the fundamental band gap (Δ_g) and green squares represent the non-trivial band gap at Γ (Δ_{ng}^Γ).

Adding SOC leads to Rashba-type splittings, however the metallic character is maintained. In order to remove the unsaturated dangling bond states, we passivate the exposed surface atoms with hydrogen and halogens (F, Cl, Br and I). We observe that the hydrogen and halogens atoms form strong bonds to the Bi atom, with binding energies varying from ~ 3.0 eV for fluorine to ~ 2.0 eV for iodine, regardless of the column-III elements. This behavior was also observed for free-standing films¹⁷. The band structures of the fluorinated surfaces are shown in Figures 2(d), (e) and (f). Without SOC, the three materials are semimetals, with the valence and conduction band touching at Γ (shaded region). When SOC is turned on, non-trivial band gaps appear. The variation of fundamental band gap (Δ_g) and non-trivial band gap (Δ_{ng}^Γ) with the passivating species X= H, F, Cl, Br, I, for AlBi, GaBi and InBi are shown in panels (g), (h), and (i). For AlBi, the fundamental band gap and the non-trivial band gap are almost the same for all halogens, except for iodine.

The topological nature of the III-Bi layers can be con-

firmed by a nonzero topological invariant Z_2 , calculated here using the WCCs method.^{30,31}. The topological invariant $Z_2=1$ were determined for all III-Bi systems, with III=Al, Ga, Bi, functionalized with H, F, Cl, Br and I. Only the results for SrTe/InBi-F are shown in Figure 3(a). By analyzing the evolution of the WCCs between two time-reversal invariant momenta (TRIM) in the Brillouin zone, we find that the WCCs always cross the red dashed line odd times, giving $Z_2=1$.

We also verified the topological nature of the band structure by inspecting the orbital-resolved electronic band structure of each material. In Figure 3(b) we show the orbital-projected band structure of SrTe/InBi-F. The projections on s (top) and p_{xy} (bottom) orbitals without SOC are shown on the left panel, where we note an s - p band inversion near the Γ point. When SOC is included, there is an opening of a gap at the Fermi level; the s state remains occupied at the valence band and the p_{xy} states are unoccupied in the conduction band. In 3(c) we show a schematic energy diagram of SrTe/InBi-F for the electronic states near the Fermi level, with and without

SOC. The unsaturated system is metallic, and the s and p_{xy} states are unoccupied. With the F atoms bonded to the Bi atoms, s states are populated and the p_{xy} orbitals are lowered to the Fermi level. When SOC is included, there is a split of the p_{xy} bonding and antibonding states, opening a non-trivial band gap at the Γ point. We have checked that the s-p band inversion is preserved when the calculations are performed using the HSE06 hybrid functional calculations^{35,36}.

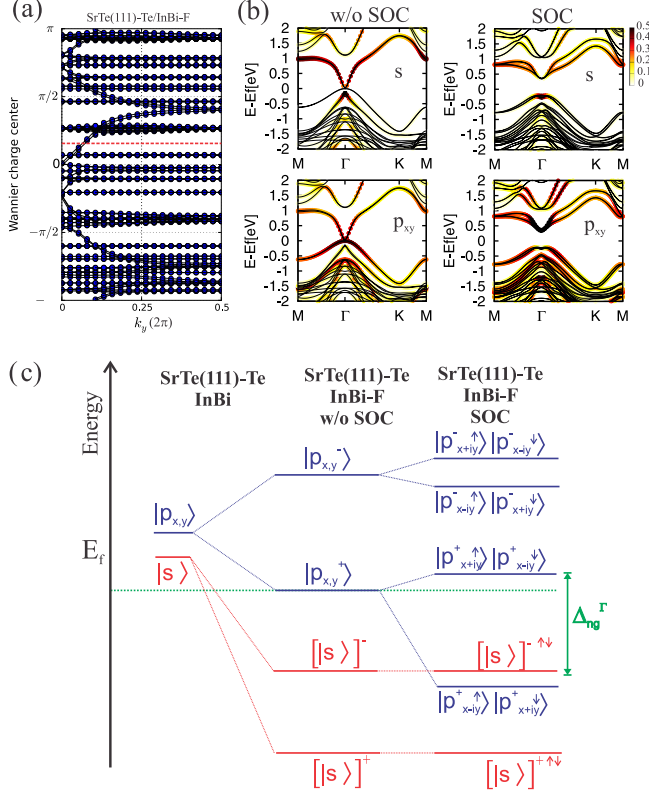


FIG. 3. (Color online) (a) Tracking of the evolution of the Wannier Charge Centers (WCCs) between two TRIM points in the reciprocal plane $k_z = 0$. In dashed red we have a reference line to track the number of Wannier center pair switching in half of the Brillouin Zone. (b) Projected band structure on s and p_{xy} orbitals of InBi-F on Te-terminated SrTe(111) substrate without SOC (left panel) and with SOC (right panel). (c) Schematic representation of the evolution of the s and p_{xy} orbitals for the conduction and valence bands, at the Γ point, of InBi-F on SrTe(111), without and with the SOC.

A key feature of 2D topological insulators is the existence of an odd number of topologically protected one-dimensional helical Dirac-like edge states. These states connect the conduction and valence bands when the 2D topological insulator is interfaced with a trivial insulator. In Figure 4 (a) we show the band structure for an armchair terminated nanoribbon with a width of ~ 10 nm, where we can clearly see the presence of Dirac-like edge states. The spacial distribution of the Dirac states, near the Γ -point, is shown in Figure 4(b) in a frontal view of the ribbon, i.e., looking at the ribbon infinite length.

The topological edge states are distributed near the edge sites and with a penetration of a few unit cells inside the InBi-F nanoribbon. The presence of states inside the SrTe substrate comes from the dangling bond states that is present due the artificially terminated SrTe substrate.

Since the edges are symmetric with respect to the center of the nanoribbon, the Dirac states are degenerate and spin-momentum locked. The the spin projection of the edge states was calculated via the spin polarization vector, $P_n(k) = \langle u_{nk}^{\sigma} | \sigma | u_{nk}^{\sigma} \rangle$, where $|u_{nk}^{\sigma}\rangle$ are the ab initio Bloch states, and $\sigma = (\sigma_x, \sigma_y, \sigma_z)$ is the Pauli matrices vector. For a δk close to the Γ point, we determined the spin projection $P_{x,n}$, $P_{y,n}$ and $P_{z,n}$, where for all states 1, 2, 3 and 4, presented in Figure 4(a), the $P_{x,n}$ and $P_{y,n}$ projections are negligible, remaining only the $P_{z,n}$ component. A similar behavior was observed by Seixas et. al for the edge states in a germanane nanoroad³⁴. The states above the Dirac point near Γ , energy bands 1 and 2 indicated in Figure 4(b), have opposite spin polarization and are localized on opposite edges of the ribbon. Furthermore, by inspecting states localized on the same edge, we find that them to exhibit opposite spin polarization, i.e., $\psi_{\Gamma-\delta k}^{\uparrow}$ and $\psi_{\Gamma+\delta k}^{\downarrow}$; thus, although lying on the same edge, backscattering processes are not allowed ($\psi_{\Gamma-\delta k}^{\uparrow} \leftrightarrow \psi_{\Gamma+\delta k}^{\downarrow}$). The same applies to bands 3 ($\psi_{\Gamma-\delta k}^{\downarrow}$) and 4 ($\psi_{\Gamma-\delta k}^{\uparrow}$), as well for the electronic states below the Dirac crossing, near the Γ -point. These are main characteristics of quantum spin Hall insulators.

Finally, we also investigated multilayer systems with 2D topological insulators, composed of 2D TI layers sandwiched between SrTe layers such as the heterostructure schematically shown in Figure 5(a). In this way, instead of passivating the top surface of the 2D InBi with H or halogen species, another layer of the SrTe is grown on top of InBi. In order to verify that the InBi layer still retains its topological properties, we explicitly simulated the heterostructure displayed in Figure 5(b). It consists of a InBi layer between 13 atomic layers of SrTe on the bottom and 10 atomic layers on top of the InBi layer. The out-of plane lattice parameter and atomic positions were fully relaxed.

The band structure of the SrTe/InBi/SrTe heterostructure, without SOC, is shown in Figure 5(c). We can see an s - p band inversion around the Fermi level. When SOC is included [see Figure 5(d)], a non-trivial band gap at Γ appears, revealing that this heterostructure is also characterized by the presence of a 2D TI, the same behavior presented by the systems with hydrogen and halogens decorating the top surface. From these results, we conclude that we can create heterostructures based on III-Bi 2D TI presenting large 2D non-trivial band gaps. This approach would be more robust, in practice, than having a free standing InBi layer, as described by other authors, or even a single layer passivated with H or halogens. We believe these results constitute a new route for the growth and use of 2D quantum spin hall insulators in practical applications. The III-Bi layers could be deposited or grown on SrTe substrate using various epitaxial growth

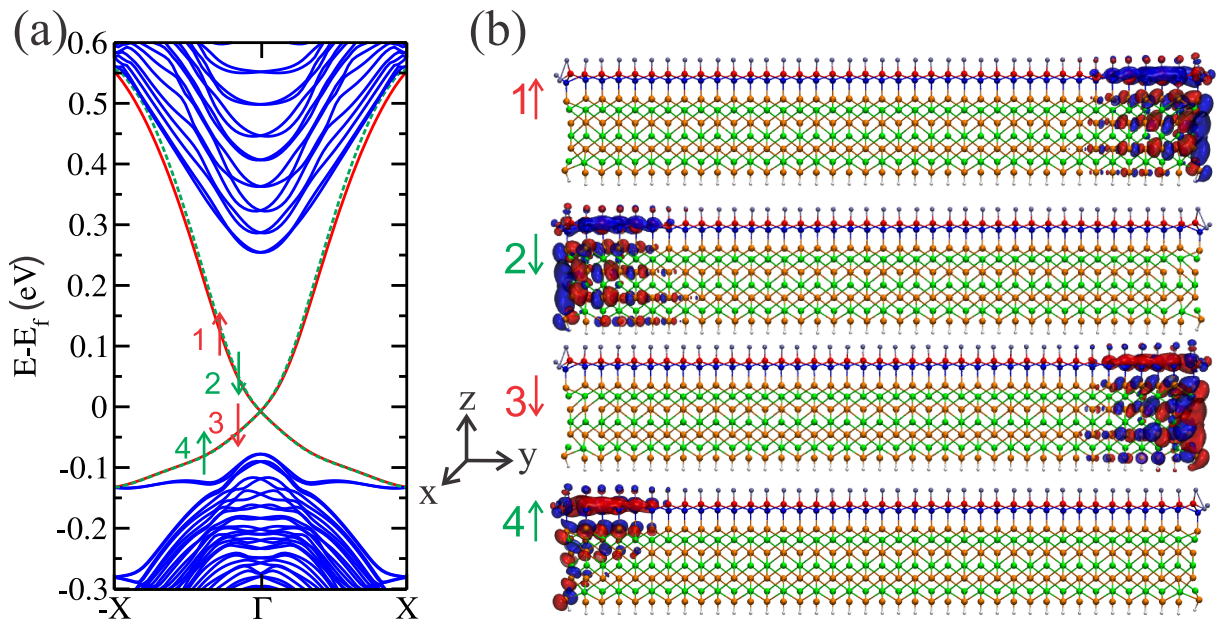


FIG. 4. (Color online) (a) Electronic band structure of an armchair InBi nanoribbon passivated with fluorine and deposited on top of a Te-terminated SrTe(111) slab. We used a finite slab composed of 7 layers of SrTe with InBi-F at the top. On the other side the dangling bonds were saturated with hydrogen atoms to prevent any surface dangling bond states. (b) Wave function for a k -point close to the Γ point for each edge state presented in (a).

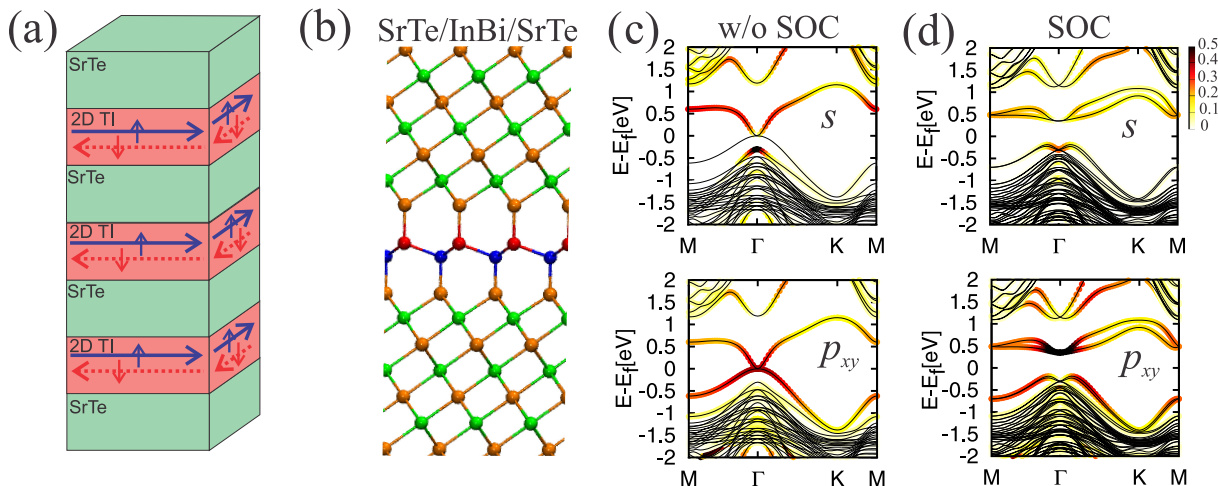


FIG. 5. (Color online) (a) Schematic representation of a heterostructure of several 2D TI grown on substrates. (b) Ball stick representation of InBi between two SrTe(111) layers. Orbital resolved band structure projected on the s and p_{xy} orbitals of InBi between SrTe (c) without SOC and (d) with SOC.

techniques, such as molecular beam epitaxy, or chemical vapor deposition. For the SrTe/III-Bi/SrTe structures, perhaps pulsed laser deposition would be more appropriate due to the flexibility regarding the number of different species present in the growth chamber, as the deposition of a SrTe top layer would be required to cap the III-Bi layer. In all, the growth or deposition will be facilitated by the small lattice mismatch between the III-Bi and the SrTe substrate, and the ultrathin layer thickness of the III-Bi layer.

III. CONCLUSIONS

In summary, we show that the III-V bismuth based 2D materials grown on the anion-terminated SrTe(111) are 2D topological insulators when the exposed surface are decorated with hydrogen or halogens. All systems studied here exhibit large non-trivial band gaps, ranging from 0.15 to 0.72 eV. Our calculations show that Γ -centered 1D Dirac helical edge states appear on the edges of nanoribbon structures, and these states are protected by time-reversal symmetry. More importantly,

when both sides of the 2D material is sandwiched by SrTe layers, the topological phases are still present, opening a new route to build devices based on 2D quantum spin hall insulators.

IV. ACKNOWLEDGEMENT

This work was supported by the Brazilian agencies FAPESP, CNPq and CAPES. AJ acknowledges finan-

cial support form U.S. DOE. We also would like to acknowledge computing time provided on the Blue Gene/Q supercomputer supported by the Research Computing Support Group (Rice University) and Laboratório de Computação Científica Avançada (Universidade de São Paulo), and the Extreme Science and Engineering Discovery Environment (XSEDE), which is supported by National Science Foundation grant number ACI-1053575. Finally, we acknowledge Dr. Soluyanov for sharing the code to calculate the wannier charge centers in the VASP code.

-
- * jose.padilha@ufpr.br
 † janotti@udel.edu
 ‡ fazzio@if.usp.br
 § jose.roque@lnls.br
- ¹ C. L. Kane and E. J. Mele, *Phys. Rev. Lett.* **95**, 226801 (2005).
 - ² H. Min, J. E. Hill, N. A. Sinitsyn, B. R. Sahu, L. Kleinman and A. H. MacDonald, *Phys. Rev. B* **74** 165310 (2006).
 - ³ Y. Yao, F. Ye, X.-L. Qi, S.-C. Zhang and Z. Fang, *Phys. Rev. B* **75**, 041401 (2007).
 - ⁴ B. A. Bernevig, T. L. Hughes, and S.-C. Zhang, *Science* **314**, 1757 (2006).
 - ⁵ A. Kara, H. Enriquez, A. P. Seitsonen, L. C. L. Y. Voon, S. Vizzini, B. Aufray and H. Oughaddou, *Surf. Sci. Rep.* **67**, 1 (2012).
 - ⁶ C. C. Liu, W. X. Feng and Y. G. Yao, *Phys. Rev. Lett.* **107**, 076802 (2011).
 - ⁷ J. E. Padilha, L. B. Abdalla, A. J. R. da Silva and A. Fazzio, *Phys. Rev. B* **93**, 045135 (2016).
 - ⁸ Y. Xu, B. Yan, H.-J. Zhang, J. Wang, G. Xu, P. Tang, W. Duan and S.-C. Zhang, *Phys. Rev. Lett.* **111**, 136804 (2013).
 - ⁹ H. Zhang, C.-X. Liu, X.-L. Qi, X. Dai, Z. Fang and S.-C. Zhang, *Nat. Phys.* **5**, 438-442 (2009).
 - ¹⁰ W. Zhang, R. Yu, H.-J. Zhang, X. Dai and Z. Fang, *New J. Phys.* **12**, 065013 (2010).
 - ¹¹ L. B. Abdalla, J. E. Padilha, T. M. Schmidt, R. H. Miwa and A. Fazzio, *J. of Phys.: Cond. Matt.* **27**, 255501 (2015).
 - ¹² E. Frantzeskakis, S. Pons and Marco Grioni, *Phys. Rev. B* **82**, 085440 (2010)
 - ¹³ D. V. Khomitsky and A. A. Chubunov, *J. Exp. Theor. Phys.* **118**, 457 (2014).
 - ¹⁴ F.-C. Chuang, L.-Z. Yao, Z.-Q. Huang, Y.-T. Liu, C.-H. Hsu, T. Das, H. Lin and A. Bansil, *Nano Lett.* **14**, 2505-2508 (2014).
 - ¹⁵ Y. Ma, X. Li, L. Kou, B. Yan, C. Niu, Y. Dai and T. Heine, *Phys. Rev. B* **91**, 235306 (2015).
 - ¹⁶ R. R. Q. Freitas, F. de Brito Mota, R. Rivelino, C. M. C. de Castilho, A. Kakanakova-Georgieva and G. K. Gueorguiev, *J. Phys. Chem. C* **119**, 23599?23606 (2015).
 - ¹⁷ R. R. Q. Freitas, F. de Brito Mota, R. Rivelino, C. M. C. de Castilho, A. Kakanakova-Georgieva and G. K. Gueorguiev, *Nanotechnology* **27**, 055704 (2016).
 - ¹⁸ J. E. Padilha, R. B. Pontes, T. M. Schmidt, R. H. Miwa and A. Fazzio, *Scientific Reports* **6**, 26123 (2016).
 - ¹⁹ Z.-Q. Huang, C.-H. Hsu, F.-C. Chuang, Y.-T. Liu, H. Lin, W.-S. Su, V. Ozolins and Arun Bansil, *New J. Phys.* **16**, 105018 (2014).
 - ²⁰ F. Zhu, W.-J. Chen, Y. Xu, C.-L. Gao, D.-D. Guan, L. Canhua, D. Qian, S.-C. Zhang, and J.-F. Jia, *J.-F. Nat. Mater.* **14**, 1020-1015 (2015).
 - ²¹ Y. Xu, P. Tang and S.-C. Zhang, *Phys. Rev. B* **92**, 081112(R) (2015).
 - ²² C. P. Crisostomo, L.-Z. Yao, Z.-Q. Huang, C.-H. Hsu, F.-C. Chuang, H. Lin, M. A. Albao and A. Bansil, *Nano Lett.* **15** 6568 (2015).
 - ²³ L.-Z. Yao, C. P. Crisostomo, C.-C. Yeh, S.-M. Lai, Z.-Q. Huang, C.-H. Hsu, F.-C. Chuang, H. Lin and A. Bansil, *Scientific Reports* **5**, 15463 (2015).
 - ²⁴ P. Hohenberg and W. Kohn *Phys. Rev.* **136**, B864 (1964).
 - ²⁵ W. Kohn and L. J. Sham, *Phys. Rev.* **140**, A1133 (1965).
 - ²⁶ J. P. Perdew, K. Burke and M. Ernzerhof, *Phys. Rev. Lett.* **77**, 3865 (1996).
 - ²⁷ G. Theurich and N. A. Hill, *Phys. Rev. B* **64**, 073106 (2001).
 - ²⁸ G. Kresse, and J. Furthmüller, *Phys. Rev. B* **54** 11169 (1996).
 - ²⁹ G. Kresse and D. Joubert, *Phys. Rev. B* **59** 1758 (1999).
 - ³⁰ A. A. Soluyanov and D. Vanderbilt, *Phys. Rev. B* **83**, 035108 (2011).
 - ³¹ A. A. Soluyanov and D. Vanderbilt, *Phys. Rev. B* **83**, 235401 (2011).
 - ³² N. Marzari, A. A. Mostofi, J. R. Yates, I. Souza and D. Vanderbilt, *Rev. Mod. Phys.* **84**, 1419 (2012).
 - ³³ T. Ozaki, *Phys. Rev. B* **67**, 155108 (2003).
 - ³⁴ L. Seixas, J. E. Padilha and A. Fazzio, *Phys. Rev. B* **89**, 195403 (2014).
 - ³⁵ J. Heyd, G. E. Scuseria and M. Ernzerhof, *J. Chem. Phys.* **118**, 8207 (2003).
 - ³⁶ J. Heyd, G. E. Scuseria and M. Ernzerhof, *J. Chem. Phys.* **124**, 219906 (2006).